China Ocean Eng., Vol. 29, No. 4, pp. 519 – 534

DOI 10.1007/s13344-015-0036-9,   ISSN 0890-5487

System Identification Modeling of Ship Manoeuvring Motion in 4 Degrees of Freedom Based on Support Vector Machines*

WANG Xue-gang (王雪刚)[a], ZOU Zao-jian (邹早建)[a, b]

YU Long (余　龙)[a, 1] and CAI Wei (蔡　韡)[c]

[a] *School of Naval Architecture, Ocean and Civil Engineering, Shanghai Jiao Tong University, Shanghai 200240, China*

[b] *State Key Laboratory of Ocean Engineering, Shanghai Jiao Tong University, Shanghai 200240, China*

[c] *Jiujiang Branch of No.707 Research Institute, China Shipbuilding Industry Corporation, Jiujiang 332000, China*

(Received 22 November 2013; received revised form 14 May 2014; accepted 26 July 2014)

ABSTRACT

Based on support vector machines, three modeling methods, i.e., white-box modeling, grey-box modeling and black-box modeling of ship manoeuvring motion in 4 degrees of freedom are investigated. With the whole-ship mathematical model for ship manoeuvring motion, in which the hydrodynamic coefficients are obtained from roll planar motion mechanism test, some zigzag tests and turning circle manoeuvres are simulated. In the white-box modeling and grey-box modeling, the training data taken every 5 s from the simulated 20°/20° zigzag test are used, while in the black-box modeling, the training data taken every 5 s from the simulated 15°/15°, 20°/20° zigzag tests and 15°, 25° turning manoeuvres are used; and the trained support vector machines are used to predict the whole 20°/20° zigzag test. Comparisons between the simulated and predicted 20°/20° zigzag tests show good predictive ability of the proposed methods. Besides, all mathematical models obtained by the proposed modeling methods are used to predict the 10°/10° zigzag test and 35° turning circle manoeuvre, and the predicted results are compared with those of simulation tests to demonstrate the good generalization performance of the mathematical models. Finally, the proposed modeling methods are analyzed and compared with each other in aspects of application conditions, prediction accuracy and computation speed. The appropriate modeling method can be chosen according to the intended use of the mathematical models and the available data needed for system identification.

Key words: *ship manoeuvring*; *4 degrees of freedom*; *system identification*; *support vector machines*

1. Introduction

For warship and other ships with low metacentric height (e.g., container ship), ship manoeuvring motion is usually accompanied by roll motion of large amplitude. The roll motion not only affects the tactical and technical performance of warship, but also has direct impacts on ship navigation safety. Investigation of ship manoeuvring motion with the influences of the roll motion being taken into

---

* The project was financially supported by the National Natural Science Foundation of China (Grant No. 51279106) and the Special Research Fund for the Doctoral Program of Higher Education of China (Grant No. 20110073110009).

1 Corresponding author. E-mail: yulone@sjtu.edu.cn

account is one of the research hotspots. Son and Nomoto (1982) investigated the sway-yaw-roll coupling motion of a container ship on the basis of captive model tests, and a 4 degrees of freedom (4-DOF) motion equation including roll motion was established in modular mathematical model. Fossen (1994) simulated the 4-DOF ship manoeuvring motion using hydrodynamic coefficients from Son and Nomoto's tests. Blanke *et al*. (1997, 2002) presented a nonlinear whole-ship mathematical model for a container ship based on the experimental results obtained with the 4-DOF roll planar motion mechanism (RPMM) facility.

The application of System Identification (SI) method based on free-running model tests or full-scale trials plays an important role in modeling of ship manoeuvring motion (ITTC, 2005). Various SI methods are applied in modeling of ship manoeuvring motion. Model reference method (Hayes, 1971), extended Kalman filter method (Abkowitz, 1980; Revestido and Velasco, 2012), maximum likelihood method (Åström and Källström, 1976), recursive prediction error method (Källström and Åström, 1981; Zhou and Blanke, 1989), least square method (Rhee *et al*., 1998), frequency domain identification method (Bhattacharyya and Haddara, 2006; Perez and Fossen, 2011), neural network (Haddara and Wang, 1999), etc. have been used to identify the hydrodynamic coefficients in the mathematical models. Among them, neural network can not only be used for parametric identification, but they are more suitable for nonlinear regression. Artificial neural network was adopted to regress the nonlinear dynamic model of a large tanker (Rajesh and Bhattacharyya, 2008); recursive neural network was applied to simulate the ship manoeuvring motion (Hess and Faller, 2000; Moreira and Guedes Soares, 2003). In the 1990s, support vector machines (SVM), a novel method of modern artificial intelligence technology, was proposed (Vapnik, 2000). Compared with neural network, SVM is directed at finite samples and has good generalization performances and global optimal extremum. By using the least squares support vector machines (LS-SVM, Luo and Zou, 2009) and ε-support vector machines (ε-SVM, Zhang and Zou, 2011), the hydrodynamic coefficients of Abkowitz model were identified.

In this paper, three modeling methods, i.e., white-box modeling, grey-box modeling and black-box modeling of ship manoeuvring motion in 4-DOF based on LS-SVM are investigated. With the nonlinear whole-ship model proposed by Blanke *et al*. (1997, 2002), 10°/10°, 15°/15°, 20°/20° zigzag tests and 15°, 25°, 35° turning circle manoeuvres are simulated. In white-box modeling and grey-box modeling, the simulation data of 20°/20° zigzag test taken every 5 s are used to train the support vectors; while in black-box modeling, the simulation data of 15°/15°, 20°/20° zigzag tests and 15°, 25° turning manoeuvres are used; and the trained support vector machines is used to predict the whole 20°/20° zigzag test. Besides, all mathematical models obtained by the proposed modeling methods are used to predict 10°/10° zigzag test and 35° turning circle manoeuvre. The predicted results are compared with those of simulation tests to demonstrate the good predictive ability and generalization performance of the mathematical models. The modeling methods are analyzed and compared with each other in aspects of application conditions, prediction accuracy and computation speed. The appropriate modeling method can be chosen according to the intended use of the mathematical models and the available data needed for system identification.

2. Mathematical Model

Generally, the 4-DOF manoeuvring motion of a surface vessel can be described by the equations in the following form (Son and Nomoto, 1982):

$$\begin{cases} m(\dot{u}-vr-x_G r^2+z_G rp)=X \\ m(\dot{v}+ur+x_G\dot{r}-z_G\dot{p})=Y \\ I_{zz}\dot{r}+mx_G(\dot{v}+ur)=N \\ I_{xx}\dot{p}-mz_G(\dot{v}+ur)=K-W\cdot\overline{GM}\cdot\phi \end{cases} \tag{1}$$

where u, v, r, and p denote the surge speed, sway speed, yaw rate and roll rate, respectively; m is the mass of the ship; I_{xx} and I_{zz} are the moments of inertia about the longitudinal and vertical axes; x_G and z_G are the longitudinal and vertical coordinates of the ship's center of gravity; X and Y are the longitudinal and lateral hydrodynamic force components; N is the hydrodynamic yaw moment; K is the roll moment; W is the weight of the ship; $\overline{GM}$ is the metacentric height; and ϕ is the roll angle.

Expanding the hydrodynamic forces and moments in Eq. (1) by Taylor series expansion, Eq. (1) can be written as (Blanke *et al.*, 1997, 2002):

$$\begin{bmatrix} m-X_{\dot{u}} & 0 & 0 & 0 \\ 0 & m-Y_{\dot{v}} & mx_G-Y_{\dot{r}} & -mz_G-Y_{\dot{p}} \\ 0 & mx_G-N_{\dot{v}} & I_{zz}-N_{\dot{r}} & -N_{\dot{p}} \\ 0 & -mz_G-K_{\dot{v}} & -K_{\dot{r}} & I_{xx}-K_{\dot{p}} \end{bmatrix}\begin{bmatrix}\dot{u}\\ \dot{v}\\ \dot{r}\\ \dot{p}\end{bmatrix}=\begin{bmatrix}f_1\\ f_2\\ f_3\\ f_4\end{bmatrix} \tag{2}$$

$$\begin{aligned} f_1 &= X_u u_a + X_{uu}u_a^2 + X_{uuu}u_a^3 + X_{vr}vr + X_{rr}r^2 + X_v v + X_{vv}v^2 + X_{v\phi}v\phi + X_\phi\phi + X_{\phi\phi}\phi^2 + X_{pp}p^2 + X_{ppu}p^2u_a \\ &\quad + X_\delta\delta + X_{\delta\delta}\delta^2 + X_{\delta u}\delta u_a + X_{\delta\delta u}\delta^2u_a + X_{v\delta}v\delta + X_{v\delta\delta}v\delta^2 + mvr + mx_Gr^2 - mz_Grp; \end{aligned} \tag{3}$$

$$\begin{aligned} f_2 &= Y_v v + Y_{vv}v^2 + Y_{v|v|}v|v| + Y_{v|r|}v|r| + Y_{vrr}vr^2 + Y_r r + Y_{r|r|}r|r| + Y_{rrr}r^3 + Y_{r|v|}r|v| + Y_{rvv}rv^2 + Y_p p + Y_{ppp}p^3 + Y_{pu}pu_a \\ &\quad + Y_{pu|pu|}pu_a|pu_a| + Y_\phi\phi + Y_{v\phi}v\phi + Y_{v\phi\phi}v\phi^2 + Y_{\phi vv}\phi v^2 + Y_0 + Y_{0u}u_a + Y_\delta\delta + Y_{\delta\delta}\delta^2 + Y_{\delta\delta\delta}\delta^3 + Y_{\delta v}\delta v + Y_{\delta vv}\delta v^2 \\ &\quad + Y_{\delta u}\delta u_a + Y_{\delta\delta u}\delta^2u_a + Y_{\delta\delta\delta u}\delta^3u_a - mur; \end{aligned} \tag{4}$$

$$\begin{aligned} f_3 &= N_v v + N_{vv}v^2 + N_{v|v|}v|v| + N_{v|r|}v|r| + N_{vrr}vr^2 + N_r r + N_{r|r|}r|r| + N_{rrr}r^3 + N_{r|v|}r|v| + N_{rvv}rv^2 + N_p p + N_{ppp}p^3 \\ &\quad + N_{pu}pu_a + N_{pu|pu|}pu_a|pu_a| + N_\phi\phi + N_{v\phi}v\phi + N_{v\phi\phi}v\phi^2 + N_{\phi vv}\phi v^2 + N_0 + N_{0u}u_a + N_\delta\delta + N_{\delta\delta}\delta^2 + N_{\delta\delta\delta}\delta^3 \\ &\quad + N_{\delta v}\delta v + N_{\delta vv}\delta v^2 + N_{\delta u}\delta u_a + N_{\delta\delta u}\delta^2u_a + N_{\delta\delta\delta u}\delta^3u_a - mx_Gur; \end{aligned} \tag{5}$$

$$\begin{aligned} f_4 &= K_v v + K_{vv}v^2 + K_{v|v|}v|v| + K_{v|r|}v|r| + K_{vrr}vr^2 + K_r r + K_{r|r|}r|r| + K_{rrr}r^3 + K_{r|v|}r|v| + K_{rvv}rv^2 + K_p p + K_{p|p|}p|p| \\ &\quad + K_{ppp}p^3 + K_{pu}pu_a + K_{pu|pu|}pu_a|pu_a| + K_{v\phi}v\phi + K_{v\phi\phi}v\phi^2 + K_{\phi vv}\phi v^2 + K_0 + K_{0u}u_a + K_\delta\delta + K_{\delta\delta}\delta^2 \\ &\quad + K_{\delta\delta\delta}\delta^3 + K_{\delta v}\delta v + K_{\delta vv}\delta v^2 + K_{\delta u}\delta u_a + K_{\delta\delta u}\delta^2u_a + K_{\delta\delta\delta u}\delta^3u_a - W\,\overline{GM}\,\phi + mz_Gur, \end{aligned} \tag{6}$$

where u_a is the relative surge speed defined as $u_a = U - U_{\mathrm{nom}}$, $U=\sqrt{u^2+v^2}$ is the ship's absolute speed, U_{nom} is the nominal speed; X_u, Y_v, N_r, K_p etc. are the hydrodynamic coefficients; δ is the rudder angle.

3. Least Square Support Vector Machines

LS-SVM is an improved type of SVM. To avoid the uncertainties in selecting structural parameters, some improvements (Suykens and Vandewalle, 1999) have been made. Because of the choice of square loss function, the sparse solution feature is lost. But it does not heavily influence the precision of the results; in contrast, it transfers the solution of quadratic optimization problem to solving a linear system of equations, which immensely saves the computational time.

The feature space representation of LS-SVM can be described as

$$y(\boldsymbol{x}) = \boldsymbol{w}^{\mathrm{T}}\Phi(\boldsymbol{x}) + b \quad (\boldsymbol{x} \in \mathbf{R}^{m_x},\ y \in \mathbf{R}^{n}) \tag{7}$$

where $y(\boldsymbol{x})$ is the scalar output of the system; $\Phi(\boldsymbol{x})$ is a high-dimensional feature space to approximate the hidden mapping contained in the original training samples; $\boldsymbol{x}$ is the input vector of the system; $\boldsymbol{w}$ is the weight matrix; b is the bias (constant); $\mathbf{R}$ is the Euclidean space; m_x and n are the dimensions of the Euclidean space.

The optimization problem is

$$\min_{w,e} J(\boldsymbol{w}, e) = \frac{1}{2}\boldsymbol{w}^{\mathrm{T}}\boldsymbol{w} + \frac{1}{2}C\sum_{i=1}^{n} e_i^2 \tag{8}$$

subject to

$$y_i = \boldsymbol{w}^{\mathrm{T}}\Phi(x_i) + b + e_i \quad (i = 1, 2, \cdots, n) \tag{9}$$

where C is the penalty factor, and e is the regression error.

The following Lagrangian function is defined for objective function and constraint conditions

$$L_{\mathrm{a}}(\boldsymbol{w}, e, \beta, b) = J(\boldsymbol{w}, e) - \sum_{i=1}^{n} \beta_i \left[\boldsymbol{w}^{\mathrm{T}}\Phi(x_i) + b + e_i - y_i\right], \tag{10}$$

where β_i is the Lagrangian multiplier.

Taking the partial derivatives of L_a with respect to $\boldsymbol{w}$, e, β and b, and setting the derivatives to be zero, respectively, we have

$$\frac{\partial L_{\mathrm{a}}}{\partial \boldsymbol{w}} = 0 \rightarrow \boldsymbol{w} = \sum_{i=1}^{n} \beta_i \Phi(x_i); \tag{11}$$

$$\frac{\partial L_{\mathrm{a}}}{\partial e_i} = 0 \rightarrow \beta_i = Ce_i; \tag{12}$$

$$\frac{\partial L_{\mathrm{a}}}{\partial \beta_i} = 0 \rightarrow \boldsymbol{w}^{\mathrm{T}}\Phi(x_i) + b + e_i - y_i = 0; \tag{13}$$

$$\frac{\partial L_{\mathrm{a}}}{\partial b} = 0 \rightarrow \sum_{i=1}^{n} \beta_i = 0. \tag{14}$$

Substituting Eqs. (11) and (12) into Eq. (13), subject to Eq. (14), gives

$$\begin{bmatrix} \mathbf{0} & \boldsymbol{E} \\ \boldsymbol{E}^{\mathrm{T}} & \Omega + C^{-1}I \end{bmatrix} \begin{bmatrix} b \\ \boldsymbol{\beta} \end{bmatrix} = \begin{bmatrix} \mathbf{0} \\ \boldsymbol{y} \end{bmatrix} \tag{15}$$

where $\boldsymbol{y}=[y_1,\cdots,y_n]^{\mathrm{T}}$, $\boldsymbol{E}=[1,\cdots,1]^{\mathrm{T}}$, $\boldsymbol{\beta}=[\beta_1,\cdots,\beta_n]^{\mathrm{T}}$, $\Omega=\Phi(x_i)^{\mathrm{T}}\Phi(x_j)=K(x_i,x_j)$, $\mathbf{0}=[0,\cdots,0]^{\mathrm{T}}$. $K(x_i,x_j)$ is the kernel function. The regression estimation function can be obtained, once Eq. (15) is solved:

$$y=\sum_{i=1}^{n}\beta_i K(x_i,x)+b\,. \tag{16}$$

4. Modeling Method

There are three kinds of system identification modeling method, i.e., white-box modeling, grey-box modeling, and black-box modeling. In white-box modeling, the motion law of the system is analyzed based on the structure of the system; the mathematical model of the system is derived. White-box modeling is also known as the mechanism modeling. Black-box modeling is a modeling method using only the input-output data of the system, even if both the structure and parameters of the system are unknown at all. Black-box modeling aims at an appropriate approximation of the actual system. Grey-box modeling is a hybrid modeling method combining the white-box modeling and black-box modeling for the system which is not fully known.

4.1 White-Box Modeling

For the purpose of parametric identification and computer simulation, the continuous equation of motion is discretized by using Euler's stepping method as:

$$\begin{cases}\dot{u}(k)=[u(k+1)-u(k)]/h\\ \dot{v}(k)=[v(k+1)-v(k)]/h\\ \dot{r}(k)=[r(k+1)-r(k)]/h\\ \dot{p}(k)=[p(k+1)-p(k)]/h\end{cases} \tag{17}$$

where h is the sampling interval, k and k+1 are the adjacent sampling time steps.

Substituting Eq. (17) into Eqs. (2)–(6), we can obtain the identification formulas in the nondimensional form as follows:

$$\begin{cases}\boldsymbol{C}_{\boldsymbol{X}_{\mathrm{w}}}\cdot\boldsymbol{X}_{\mathrm{w}}=L^2\left[\left(m'-X'_{\dot{u}}\right)\dfrac{u(k+1)-u(k)}{LhU^2(k)}-m'\dfrac{v(k)r(k)}{LU^2(k)}-m'x'_G\dfrac{r^2(k)}{U^2(k)}+m'z'_G\dfrac{r(k)p(k)}{U^2(k)}\right]\\ \boldsymbol{C}_{\boldsymbol{Y}_{\mathrm{w}}}\cdot\boldsymbol{Y}_{\mathrm{w}}=L^2\left[\left(m'-Y'_{\dot{v}}\right)\dfrac{v(k+1)-v(k)}{LhU^2(k)}+\left(m'x'_G-Y'_{\dot{r}}\right)\dfrac{r(k+1)-r(k)}{hU^2(k)}+\left(-m'z'_G-Y'_{\dot{p}}\right)\dfrac{p(k+1)-p(k)}{hU^2(k)}+m'\dfrac{u(k)r(k)}{LU^2(k)}\right]\\ \boldsymbol{C}_{\boldsymbol{N}_{\mathrm{w}}}\cdot\boldsymbol{N}_{\mathrm{w}}=L^2\left[\left(m'x'_G-N'_{\dot{v}}\right)\dfrac{v(k+1)-v(k)}{LhU^2(k)}+\left(I'_{zz}-N'_{\dot{r}}\right)\dfrac{r(k+1)-r(k)}{hU^2(k)}+\left(-N'_{\dot{p}}\right)\dfrac{p(k+1)-p(k)}{hU^2(k)}+m'x'_G\dfrac{u(k)r(k)}{LU^2(k)}\right]\\ \boldsymbol{C}_{\boldsymbol{K}_{\mathrm{w}}}\cdot\boldsymbol{K}_{\mathrm{w}}=L^2\left[\left(-m'z'_G-K'_{\dot{v}}\right)\dfrac{v(k+1)-v(k)}{LhU^2(k)}+\left(-K'_{\dot{r}}\right)\dfrac{r(k+1)-r(k)}{hU^2(k)}+\left(I'_{xx}-K'_{\dot{p}}\right)\dfrac{p(k+1)-p(k)}{hU^2(k)}-m'z'_G\dfrac{u(k)r(k)}{LU^2(k)}\right]\\ \qquad +W'\overline{GM'}\phi(k)\end{cases} \tag{18}$$

where coefficient vectors $\boldsymbol{C}_{\boldsymbol{X}_{\mathrm{w}}}$, $\boldsymbol{C}_{\boldsymbol{Y}_{\mathrm{w}}}$, $\boldsymbol{C}_{\boldsymbol{N}_{\mathrm{w}}}$, and $\boldsymbol{C}_{\boldsymbol{K}_{\mathrm{w}}}$ and variable vectors $\boldsymbol{X}_{\mathrm{w}}$, $\boldsymbol{Y}_{\mathrm{w}}$, $\boldsymbol{N}_{\mathrm{w}}$, and $\boldsymbol{K}_{\mathrm{w}}$ are given as:

$$\boldsymbol{C}_{X_{\mathrm{w}}} = \left[X'_u, X'_{uu}, X'_{uuu}, X'_{vr} + m', X'_{rr} + m'x'_G, X'_v, X'_{vv}, X'_{v\phi}, X'_{\phi}, X'_{\phi\phi}, X'_{pp}, X'_{ppu}, X'_{\delta}, X'_{\delta\delta}, X'_{\delta u}, X'_{\delta\delta u}, X'_{v\delta}, X'_{v\delta\delta} \right]_{1\times18};$$

$$\boldsymbol{C}_{Y_{\mathrm{w}}} = \left[Y'_v, Y'_{vv}, Y'_{v|v|}, Y'_{v|r|}, Y'_{vrr}, Y'_r, Y'_{r|r|}, Y'_{rrr}, Y'_{r|v|}, Y'_{rvv}, Y'_p, Y'_{ppp}, Y'_{pu}, Y'_{pu|pu|}, Y'_{\phi}, Y'_{v\phi}, Y'_{v\phi\phi}, Y'_{\phi vv}, Y'_0, Y'_{0u}, Y'_{\delta}, Y'_{\delta\delta}, Y'_{\delta\delta\delta}, Y'_{\delta v}, Y'_{\delta vv}, Y'_{\delta u}, Y'_{\delta\delta u}, Y'_{\delta\delta\delta u} \right]_{1\times28};$$

$$\boldsymbol{C}_{N_{\mathrm{w}}} = \left[N'_v, N'_{vv}, N'_{v|v|}, N'_{v|r|}, N'_{vrr}, N'_r, N'_{r|r|}, N'_{rrr}, N'_{r|v|}, N'_{rvv}, N'_p, N'_{ppp}, N'_{pu}, N'_{pu|pu|}, N'_{\phi}, N'_{v\phi}, N'_{v\phi\phi}, N'_{\phi vv}, N'_0, N'_{0u}, N'_{\delta}, N'_{\delta\delta}, N'_{\delta\delta\delta}, N'_{\delta v}, N'_{\delta vv}, N'_{\delta u}, N'_{\delta\delta u}, N'_{\delta\delta\delta u} \right]_{1\times28};$$

$$\boldsymbol{C}_{K_{\mathrm{w}}} = \left[K'_v, K'_{vv}, K'_{v|v|}, K'_{v|r|}, K'_{vrr}, K'_{r|r|}, K'_{rrr}, K'_{r|v|}, K'_{rvv}, K'_p, K'_{p|p|}, K'_{ppp}, K'_{pu}, K'_{pu|pu|}, K'_{v\phi}, K'_{v\phi\phi}, K'_{\phi vv}, K'_0, K'_{0u}, K'_r, K'_{\delta}, K'_{\delta\delta}, K'_{\delta\delta\delta}, K'_{\delta v}, K'_{\delta vv}, K'_{\delta u}, K'_{\delta\delta u}, K'_{\delta\delta\delta u} \right]_{1\times28};$$

$$\boldsymbol{X}_{\mathrm{w}} = \left[u_a(k), u_a^2(k), u_a^3(k), v(k)r(k), r^2(k), v(k), v^2(k), v(k)\phi(k), \phi(k), \phi^2(k), p^2(k), p^2(k)u_a(k), \delta(k), \delta^2(k), \delta(k)u_a(k), \delta^2(k)u_a(k), v(k)\delta(k), v(k)\delta^2(k) \right]^{\mathrm{T}}_{1\times18};$$

$$\boldsymbol{Y}_{\mathrm{w}} = \left[v(k), v^2(k), v(k)\left|v(k)\right|, v(k)\left|r(k)\right|, v(k)r^2(k), r(k), r(k)\left|r(k)\right|, r^3(k), r(k)\left|v(k)\right|, r(k)v^2(k), p(k), p^3(k), p(k)u_a(k), p(k)u_a(k)\left|p(k)u_a(k)\right|, \phi(k), v(k)\phi(k), v(k)\phi^2(k), \phi(k)v^2(k), 1, u_a(k), \delta(k), \delta^2(k), \delta^3(k), \delta(k)v(k), \delta(k)v^2(k), \delta(k)u_a(k), \delta^2(k)u_a(k), \delta^3(k)u_a(k) \right]^{\mathrm{T}}_{1\times28};$$

$$\boldsymbol{N}_{\mathrm{w}} = \left[v(k), v^2(k), v(k)\left|v(k)\right|, v(k)\left|r(k)\right|, v(k)r^2(k), r(k), r(k)\left|r(k)\right|, r^3(k), r(k)\left|v(k)\right|, r(k)v^2(k), p(k), p^3(k), p(k)u_a(k), p(k)u(k)\left|p(k)u_a(k)\right|, \phi(k), v(k)\phi(k), v(k)\phi^2(k), \phi(k)v^2(k), 1, u_a(k), \delta(k), \delta^2(k), \delta^3(k), \delta(k)v(k), \delta(k)v^2(k), \delta(k)u_a(k), \delta^2(k)u_a(k), \delta^3(k)u_a(k) \right]^{\mathrm{T}}_{1\times28};$$

$$\boldsymbol{K}_{\mathrm{w}} = \left[v(k), v^2(k), v(k)\left|v(k)\right|, v(k)\left|r(k)\right|, v(k)r^2(k), r(k), r(k)\left|r(k)\right|, r^3(k), r(k)\left|v(k)\right|, r(k)v^2(k), p(k), p(k)\left|p(k)\right|, p^3(k), p(k)u_a(k), p(k)u_a(k)\left|p(k)u_a(k)\right|, v(k)\phi(k), v(k)\phi^2(k), \phi(k)v^2(k), 1, u(k), \delta(k), \delta^2(k), \delta^3(k), \delta(k)v(k), \delta(k)v^2(k), \delta(k)u_a(k), \delta^2(k)u_a(k), \delta^3(k)u_a(k) \right]^{\mathrm{T}}_{1\times28}.$$

The above coefficient vectors can be identified by using LS-SVM. By selecting the linear kernel function $K(x, x') = (x\, x')$, Eq. (16) is rewritten as:

$$y = \sum_{i=1}^{n} \beta_i\, x_i x + b. \tag{19}$$

According to Eq. (19), if LS-SVM has approximated the objective function well, $\sum_{i=1}^{n} \beta_i\, x_i$ are considered as the identified hydrodynamic coefficients.

The process of white-box modeling and prediction of ship manoeuvring motion by using LS-SVM is depicted in Fig. 1.

4.2 Grey-Box Modeling

By substituting Eq. (17) into Eqs. (2)–(6), the output at k+1 time step can be rearranged as:

$$\begin{cases} u(k+1) = \boldsymbol{C}_{X_\mathrm{g}} \cdot \boldsymbol{X}_\mathrm{g} \\ v(k+1) = \boldsymbol{C}_{Y_\mathrm{g}} \cdot \boldsymbol{Y}_\mathrm{g} \\ r(k+1) = \boldsymbol{C}_{N\mathrm{g}} \cdot \boldsymbol{N}_\mathrm{g} \\ p(k+1) = \boldsymbol{C}_{K_\mathrm{g}} \cdot \boldsymbol{K}_\mathrm{g} \end{cases} \tag{20}$$

where coefficient vectors $\boldsymbol{C}_{X_\mathrm{g}}$, $\boldsymbol{C}_{Y_\mathrm{g}}$, $\boldsymbol{C}_{N\mathrm{g}}$, and $\boldsymbol{C}_{K_\mathrm{g}}$ and variable vectors $\boldsymbol{X}_\mathrm{g}$, $\boldsymbol{Y}_\mathrm{g}$, $\boldsymbol{N}_\mathrm{g}$, and $\boldsymbol{K}_\mathrm{g}$ are

$\boldsymbol{C}_{X_\mathrm{g}} = [a_1, a_2, \ldots, a_{19}]_{1\times19}$, $\boldsymbol{C}_{Y_\mathrm{g}} = [b_1, b_2, \ldots, b_{29}]_{1\times29}$, $\boldsymbol{C}_{N_\mathrm{g}} = [c_1, c_2, \ldots, c_{29}]_{1\times29}$, $\boldsymbol{C}_{K_\mathrm{g}} = [d_1, d_2, \ldots, d_{29}]_{1\times29}$,

$$\boldsymbol{X}_\mathrm{g} = [u_a(k), u_a^2(k), u_a^3(k), v(k)r(k), r^2(k), v(k), v^2(k), v(k)\phi(k), \phi(k), \phi^2(k), p^2(k), p^2(k)u_a(k), \delta(k), \delta^2(k), \delta(k)u_a(k), \delta^2(k)u_a(k), v(k)\delta(k), v(k)\delta^2(k), r(k)p(k)]_{1\times19}^\mathrm{T};$$

$$\boldsymbol{Y}_\mathrm{g} = [v(k), v^2(k), v(k)|v(k)|, v(k)|r(k)|, v(k)r^2(k), r(k), r(k)|r(k)|, r^3(k), r(k)|v(k)|, r(k)v^2(k), p(k), p^3(k), p(k)u_a(k), p(k)u_a(k)|p(k)u_a(k)|, \phi(k), v(k)\phi(k), v(k)\phi^2(k), \phi(k)v^2(k), 1, u_a(k), \delta(k), \delta^2(k), \delta^3(k), \delta(k)v(k), \delta(k)v^2(k), \delta(k)u_a(k), \delta^2(k)u_a(k), \delta^3(k)u_a(k), u(k)r(k)]_{1\times29}^\mathrm{T};$$

$\boldsymbol{N}_\mathrm{g} = \boldsymbol{Y}_\mathrm{g}$; $\boldsymbol{K}_\mathrm{g} = \boldsymbol{Y}_\mathrm{g}$.

The process of grey-box modeling and prediction of ship manoeuvring motion by using LS-SVM is depicted in Fig. 2.

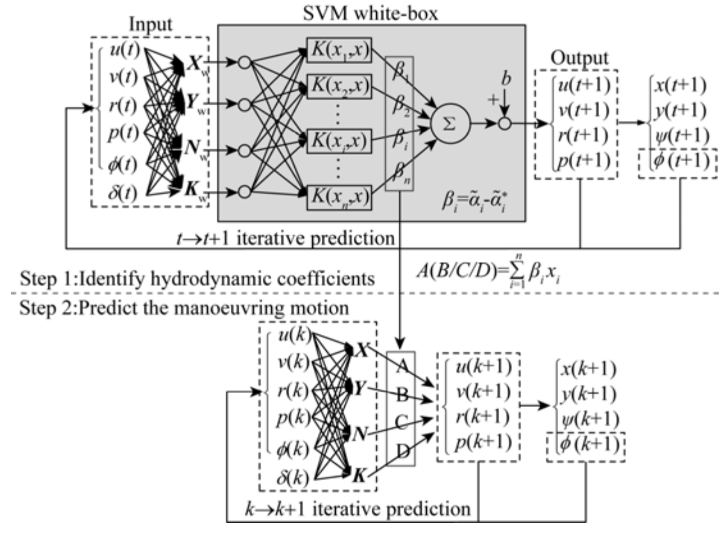

Fig. 1. Process of white-box modeling and motion prediction by using LS-SVM.

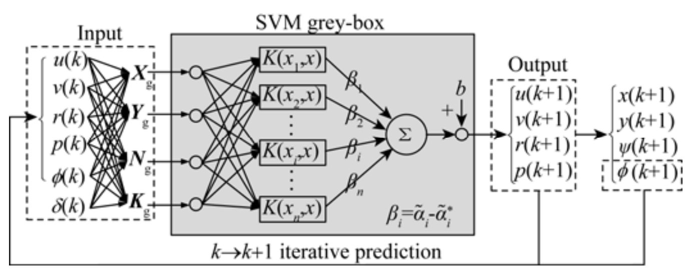

Fig. 2. Process of grey-box modeling and motion prediction by using LS-SVM.

4.3 Black-Box Modeling

From Eq. (20), it can be seen that $u(k+1)$, $v(k+1)$, $r(k+1)$, and $p(k+1)$ are the functions of $u(k)$, $v(k)$, $r(k)$, $p(k)$, $\phi(k)$, and $\delta(k)$. These equations can be rewritten as:

$$\begin{cases} u(k+1) = g_1\left[u(k), v(k), r(k), p(k), \phi(k), \delta(k)\right] \\ v(k+1) = g_2\left[u(k), v(k), r(k), p(k), \phi(k), \delta(k)\right] \\ r(k+1) = g_3\left[u(k), v(k), r(k), p(k), \phi(k), \delta(k)\right] \\ p(k+1) = g_4\left[u(k), v(k), r(k), p(k), \phi(k), \delta(k)\right] \end{cases} \tag{21}$$

The process of black-box modeling and prediction of ship manoeuvring motion by using LS-SVM is depicted in Fig. 3.

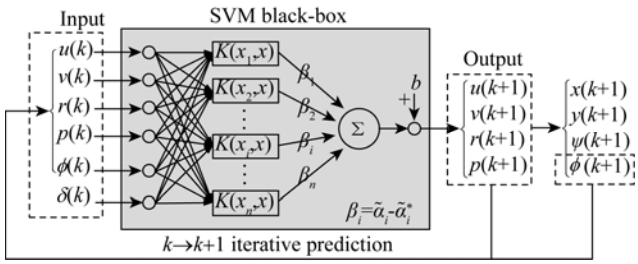

Fig. 3. Process of black-box modeling and motion prediction by using LS-SVM.

5. Prediction and Generalization Verification

5.1 Prediction

A model of container ship (Blanke *et al*., 1997, 2002) is taken as the study object. The principal dimensions of the ship are given in Table 1.

Table 1 Principal dimensions of the container ship

Parameter	Magnitude	Parameter	Magnitude
Length (L)	230.66 m	x-coordinate of CG (x_G)	–0.46 m
Beam (B)	32 m	z-coordinate of CG (z_G)	–3.54 m
Draught (D)	10.7 m	Metacentric height ($\overline{GM}$)	0.83 m
Displacement volume (∇)	46070 m^3	Block coefficient (C_B)	0.56
Non-dimensional mass (m')	750.81×10^{-5}	Propeller diameter (D_p)	8 m
Non-dimensional inertia in roll (I'_{xx})	1.30×10^{-5}	Rudder rate ($\dot{\delta}_{max}$)	2.3 °/s
Non-dimensional inertia in yaw (I'_{zz})	43.25×10^{-5}	Nominal speed (U_{nom})	12.7 m/s

Firstly, 10°/10°, 15°/15°, 20°/20° zigzag tests and 15°, 25°, 35° turning circle manoeuvres are simulated by using the hydrodynamic coefficients obtained from RPMM test (Blanke *et al*., 1997, 2002), as given in Table 2. The simulation sampling interval is 0.05 s. Surge speed u, sway speed v, yaw rate r, roll rate p etc. are obtained from the simulation.

Table 2 Comparison of identified nondimensional hydrodynamic coefficients ($\times 10^{-5}$) with RPMM test data

Accel. -coef.	RPMM	X -coef.	RPMM	Identified	Y -coef.	RPMM	Identified	N -coef.	RPMM	Identified	K -coef.	RPMM	Identified
$X'_{\dot{u}}$	–124.4	X'_{v}	–24.0	–24.0	Y'_{v}	–725.0	–725.0	N'_{v}	–300.0	–300.0	K'_{v}	25.0	25.0
$Y'_{\dot{v}}$	–878.0	X'_{vv}	–1.0	–0.9	Y'_{vv}	98.6	98.6	N'_{vv}	–0.6	–0.6	K'_{vv}	0.0	0.0
$Y'_{\dot{r}}$	–48.1	X'_{δ}	–1.4	–1.4	$Y'_{v\|v\|}$	–5801.5	–5801.7	$N'_{v\|v\|}$	–712.9	–712.9	$K'_{v\|v\|}$	99.2	99.2
$Y'_{\dot{p}}$	23.3	$X'_{\delta\delta}$	–116.8	–116.8	Y'_{δ}	248.1	248.1	N'_{δ}	–128.9	–128.9	K'_{δ}	–6.5	–6.5
$N'_{\dot{v}}$	42.3	X'_{u}	–226.2	–226.1	$Y'_{\delta\delta}$	13.4	13.4	$N'_{\delta\delta}$	–11.9	–11.9	$K'_{\delta\delta}$	–0.8	–0.8
$N'_{\dot{r}}$	–30.0	X'_{uu}	–64.5	–63.3	$Y'_{\delta\delta\delta}$	–193.0	–193.1	$N'_{\delta\delta\delta}$	101.4	101.4	$K'_{\delta\delta\delta}$	4.1	4.1
$N'_{\dot{p}}$	0.2	X'_{uuu}	–137.2	–124.2	$Y'_{\delta u}$	–379.4	–379.4	$N'_{\delta u}$	196.9	196.9	$K_{\delta u}$	8.9	8.9
$K'_{\dot{v}}$	0.0	$X'_{v\delta}$	124.5	124.4	$Y'_{\delta\delta u}$	–55.6	–55.6	$N'_{\delta\delta u}$	12.8	12.8	$K'_{\delta\delta u}$	1.3	1.3
$K'_{\dot{r}}$	–1.0	$X'_{v\delta\delta}$	–341.0	–340.9	$Y'_{\delta\delta\delta u}$	232.3	231.9	$N'_{\delta\delta\delta u}$	–125.4	–125.2	$K'_{\delta\delta\delta u}$	–4.8	–4.8
$K'_{\dot{p}}$	–0.7	$X'_{\delta u}$	–17.2	–17.2	Y'_{0}	4.7	5.0	N'_{0}	–0.6	–0.6	K'_{0}	–0.1	–0.1
		$X'_{\delta\delta u}$	224.9	224.8	Y'_{0u}	–5.3	–5.9	N'_{0u}	6.5	6.5	K'_{0u}	1.1	1.1
		X'_{ϕ}	–5.9	–5.9	$Y'_{\delta v}$	–100.0	–100.0	$N'_{\delta v}$	–24.6	–24.6	$K'_{\delta v}$	5.4	5.4
		$X'_{\phi\phi}$	–42.2	–42.2	$Y'_{\delta vv}$	189.2	190.2	$N'_{\delta vv}$	–349.1	–349.1	$K'_{\delta vv}$	–0.9	–0.9
		$X'_{v\phi}$	108.1	108.1	Y'_{ϕ}	37.7	37.7	N'_{ϕ}	–17.9	–17.9	$K'_{p\|p\|}$	–1.0	–1.0
		X'_{rr}	4.4	4.5	$Y'_{v\phi}$	144.9	144.9	$N'_{\phi\phi}$	17.8	17.8	$K'_{v\phi}$	–14.7	–14.7
		X'_{vr}	–24.0	–24.0	$Y'_{v\phi\phi}$	2459.3	2458.0	$N'_{v\phi\phi}$	–0.9	–0.8	$K'_{v\phi\phi}$	–103.9	–103.9
		X'_{pp}	7.2	7.2	$Y'_{\phi vv}$	177.2	180.6	$N'_{\phi vv}$	–933.9	–934.0	$K'_{\phi vv}$	–6.2	–6.3
		X'_{ppu}	3.9	4.0	Y'_{r}	118.2	118.2	N'_{r}	–290.0	–290.0	K'_{r}	0.8	0.8
					$Y'_{r\|r\|}$	0	0	$N'_{r\|r\|}$	0.0	0.0	$K'_{r\|r\|}$	–20.0	–20.0
					Y'_{rrr}	–158.0	–156.9	N'_{rrr}	–224.5	–224.2	K'_{rrr}	0.0	0.0
					$Y'_{r\|v\|}$	–409.4	–409.5	$N'_{r\|v\|}$	–778.8	–778.7	$K'_{r\|v\|}$	41.1	41.1
					Y'_{rvv}	–994.6	–995.3	N'_{rvv}	–1287.2	–1286.8	K'_{rvv}	–34.6	–34.6
					$Y'_{v\|r\|}$	–1192.7	–1192.7	$N'_{v\|r\|}$	–174.7	–174.7	$K'_{v\|r\|}$	10.4	10.4
					Y'_{vrr}	–1107.9	–1107.4	N'_{vrr}	36.8	37.4	K'_{vrr}	22.2	22.2
					Y'_{p}	–3.4	–3.4	N'_{p}	–8.0	–8.0	K'_{p}	–3.0	–3.0
					Y'_{ppp}	–9.3	–9.3	N'_{ppp}	0.0	0	K'_{ppp}	0.0	0.0
					Y'_{pu}	23.6	23.6	N'_{pu}	12.8	12.8	K'_{pu}	0.0	0.0
					$Y'_{pu\|pu\|}$	–52.5	–59.9	$N'_{pu\|pu\|}$	0.0	1.3	$K'_{pu\|pu\|}$	0.0	0.2

In white-box modeling and grey-box modeling, the training samples are taken from the simulation data of 20°/20° zigzag test every 5 s. In the process of identification, the linear kernel function is selected, and penalty factor $C=10^6$ is chosen. For white-box modeling, the training sample couples consist of:

Input: $\left[\boldsymbol{X}_{\mathrm{w}}, \boldsymbol{Y}_{\mathrm{w}}, \boldsymbol{N}_{\mathrm{w}}, \boldsymbol{K}_{\mathrm{w}}\right]$

Output: $$L^2\left[\left(m'-X'_{\dot{u}}\right)\frac{u(k+1)-u(k)}{LhU^2(k)}-m'\frac{v(k)r(k)}{LU^2(k)}-m'x'_G\frac{r^2(k)}{U^2(k)}+m'z'_G\frac{r(k)p(k)}{U^2(k)}\right];$$

$$L^2\left[\left(m'-Y'_{\dot{v}}\right)\frac{v(k+1)-v(k)}{LhU^2(k)}+\left(m'x'_G-Y'_{\dot{r}}\right)\frac{r(k+1)-r(k)}{hU^2(k)}+\left(-m'z'_G-Y'_{\dot{p}}\right)\frac{p(k+1)-p(k)}{hU^2(k)}+m'\frac{u(k)r(k)}{LU^2(k)}\right];$$

$$L^2\left[\left(m'x'_G - N'_{\dot{v}}\right)\frac{v(k+1)-v(k)}{LhU^2(k)} + \left(I'_{zz} - N'_{\dot{r}}\right)\frac{r(k+1)-r(k)}{hU^2(k)} + \left(-N'_{\dot{p}}\right)\frac{p(k+1)-p(k)}{hU^2(k)} + m'x'_G\frac{u(k)r(k)}{LU^2(k)}\right];$$

$$L^2\left[\left(-m'z'_G - K'_{\dot{v}}\right)\frac{v(k+1)-v(k)}{LhU^2(k)} + \left(-K'_{\dot{r}}\right)\frac{r(k+1)-r(k)}{hU^2(k)} + \left(I'_{xx} - K'_{\dot{p}}\right)\frac{p(k+1)-p(k)}{hU^2(k)} - m'z'_G\frac{u(k)r(k)}{LU^2(k)}\right]$$
$$+W'\overline{GM'}\phi(k).$$

The hydrodynamic coefficient vectors are identified by Eq. (19) and the results are given in Table 2 in comparison with the RPMM test data. Note that the acceleration coefficients are not identified. They are treated as known constants during identification.

It can be seen from Table 2 that the identification results of the hydrodynamic coefficients are in good agreement with the RPMM test data. This shows that the proposed white-box modeling by using LS-SVM is an effective method to identify the hydrodynamic coefficients.

In the grey-box modeling, the training sample couples consist of

Input: $\left[\boldsymbol{X}_g, \boldsymbol{Y}_g, \boldsymbol{N}_g, \boldsymbol{K}_g\right]$

Output: $\left[u(k+1),\, v(k+1),\, r(k+1),\, p(k+1)\right]$

In order to make Eq. (21) have the same nonlinear mapping capability as Eq. (20), the kernel function of the black-box modeling must be nonlinear. The RBF kernel function, one of the commonly used nonlinear functions, $K(x,x') = \exp\left(-\|x-x'\|^2/(2\sigma^2)\right)$ is chosen, where σ is the width parameter which is taken as 30. SVM has a strong ability to learn from a small sample compared with neural networks, however, the sample is required to fully reflect the input and output mappings. The roll rate changes more rapidly than surge speed, sway speed and yaw rate, it is difficult to achieve better forecasting results only relying on a certain motion (such as a zigzag test or a turning circle manoeuvre). Refer to the simulation of ship motion using recurrent neural network (Hess and Faller, 2000), the training samples are taken from the simulation data of 15°/15°, 20°/20° zigzag tests and 15°, 25° turning circle manoeuvres every 5 s. The training sample couples consist of

Input: $\left[u(k), v(k), r(k), p(k), \phi(k), \delta(k)\right]$

Output: $\left[u(k+1),\, v(k+1),\, r(k+1),\, p(k+1)\right]$

Comparisons of the hydrodynamic forces and moments predicted from white-box modeling with simulated results are depicted in Fig. 4. Fig. 5 shows the comparisons of the predicted motions using the mathematical models obtained by white-box modeling, grey-box modeling, and black-box modeling with those of simulation. A satisfactory agreement demonstrates the validity of the proposed modeling methods.

5.2 Generalization Verification

To verify the generalization performance of the proposed methods using white-box modeling, grey-box modeling, and black-box modeling, 10°/10° zigzag test and 35° turning circle manoeuvre are predicted.

Comparisons of the hydrodynamic forces and moments predicted from white-box modeling with simulated results are depicted in Fig. 6 and Fig. 8. Comparisons of the predicted motions with simulated results are shown in Fig. 7 and Fig. 9. As it can be seen from these figures, good agreements are achieved, which demonstrates that all the modeling methods have a good generalization capability.

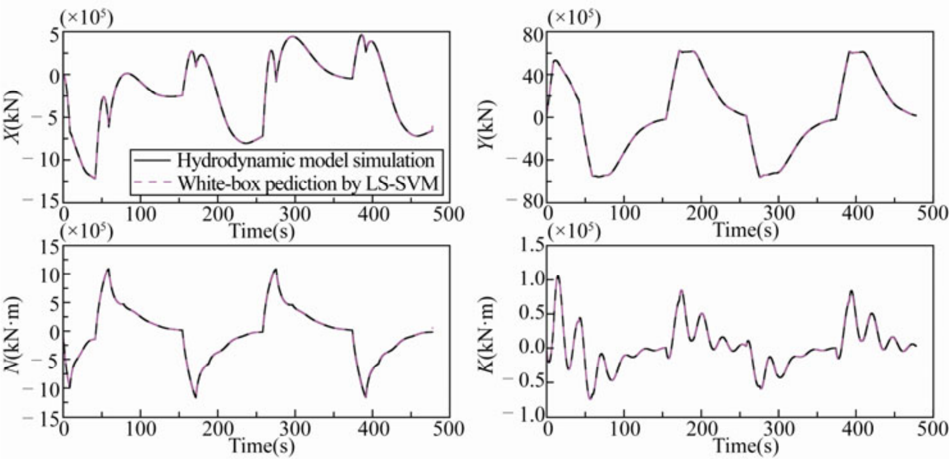

Fig. 4. Comparisons of the predicted hydrodynamic forces and moments with simulated results, 20°/20° zigzag test.

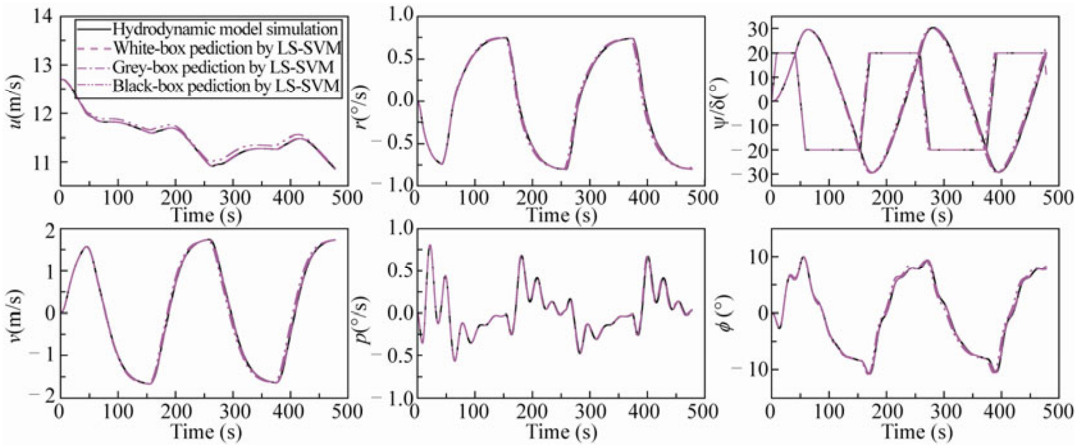

Fig. 5. Comparisons of the predicted motions with simulated results, 20°/20° zigzag test.

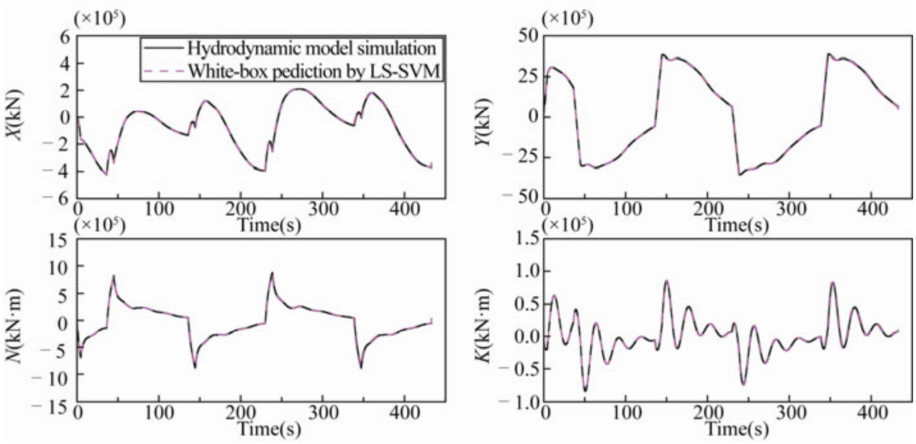

Fig. 6. Comparisons of the predicted hydrodynamic forces and moments with simulated results, 10°/10° zigzag test.

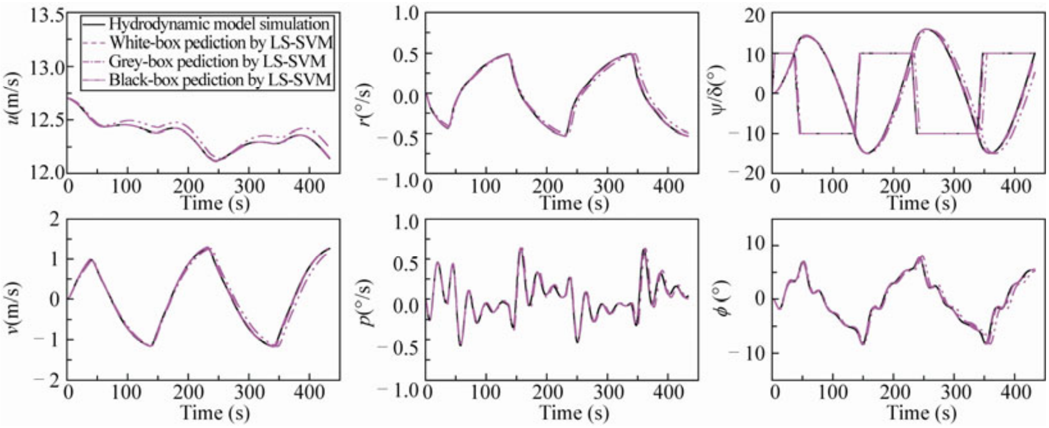

Fig. 7. Comparisons of the predicted motions with simulated results, 10°/10° zigzag test.

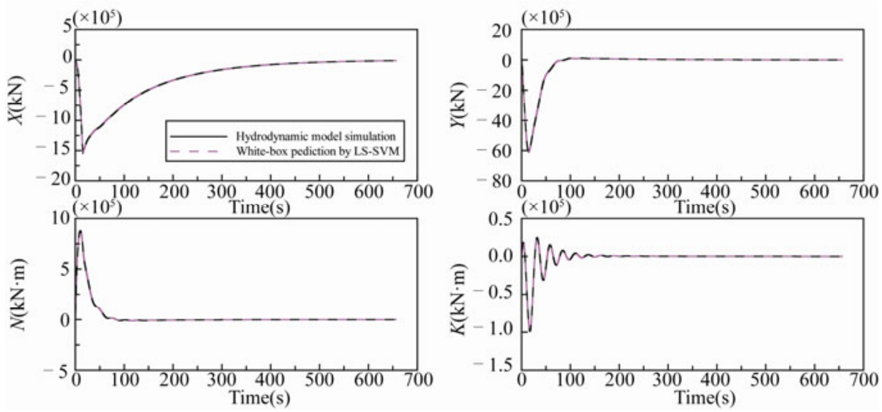

Fig. 8. Comparisons of the predicted hydrodynamic forces and moments with simulated results, 35° turning circle manoeuvre.

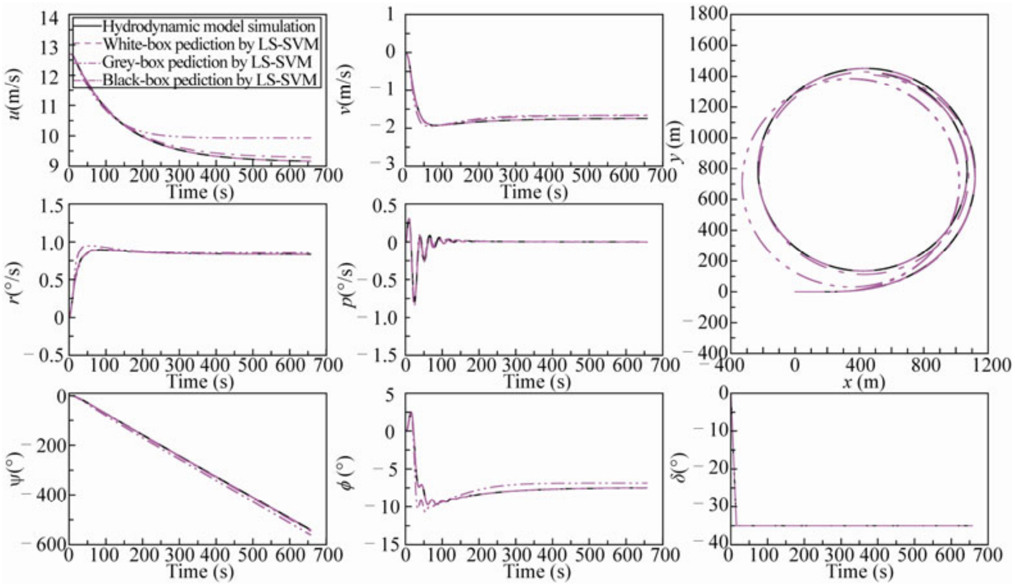

Fig. 9. Comparisons of the predicted motions with simulated results, 35° turning circle manoeuvre.

6. Comparison of the Modeling Methods

6.1 Required Known Conditions and Outputs

Requirements on the known conditions and the output results of the three modeling methods are listed in Table 3. According to the intended use of the mathematical models and the available data needed for system identification, the appropriate modeling method can be chosen. If the hydrodynamic coefficients are to be determined, only white-box modeling should be chosen; the hydrodynamic forces and moments can be predicted by white-box modeling from Eqs. (3)–(6); however, much more known data are required. When only the structures of the equations of ship manoeuvring motion are known, the grey-box modeling is a better choice. When neither the principal ship parameters, nor the structures of the equations of ship manoeuvring motion are known, black-box modeling is the only choice for modeling of ship manoeuvring motion.

Table 3 Requirements on the known conditions and the outputs of the modeling methods

Method	Requirements on known conditions	Outputs
White-box modeling	Mathematical model of ship motion Principal ship parameters: m, L, x_G etc. Acceleration coefficients: $X'_{\dot{u}}, Y'_{\dot{v}}, N'_{\dot{r}}, K'_{\dot{p}}$ etc. Motion parameters: $u(k), v(k), r(k)$ and $p(k)$ Rudder angle and roll angle: $\delta(k)$ and $\phi(k)$	Hydrodynamic coefficients: X'_u, Y'_v, N'_r, K'_p etc Hydrodynamic forces and moments: X, Y, N and K Motion parameters: $u(k+1), v(k+1), r(k+1)$ and $p(k+1)$
Grey-box modeling	Mathematical model of ship motion Motion parameters: $u(k), v(k), r(k)$ and $p(k)$ Rudder angle and roll angle: $\delta(k)$ and $\phi(k)$	Motion parameters: $u(k+1), v(k+1), r(k+1)$ and $p(k+1)$
Black-box modeling	Motion parameters: $u(k), v(k), r(k)$ and $p(k)$ Rudder angle and roll angle: $\delta(k)$ and $\phi(k)$	Motion parameters: $u(k+1), v(k+1), r(k+1)$ and $p(k+1)$

6.2 Comparison of Prediction Accuracy

Usually, Mean Square Error (MSE) and Correlation Coefficient (CC) are two evaluation criterions used to measure the prediction accuracy. All the predictions using the mathematical models obtained by the proposed modeling methods are carried out in the same computational environment. The MSE and CC of u, v, r and p are listed in Table 4.

Table 4 demonstrates that all the proposed modeling methods have high prediction accuracy. However, the accuracy of white-box modeling and grey-box modeling is significantly higher than that of black-box modeling. The reason is that the inputs of white-box modeling and grey-box modeling are both high-dimensional vectors and hence can better reflect the system characteristics; while the input of black-box modeling is only one-dimensional vector. White-box modeling and grey-box modeling have a stronger nonlinear mapping ability than black-box modeling, although the RBF kernel function is chosen in black-box modeling.

6.3 Comparison of Prediction Speed

The training time and prediction time per step of each manoeuvre are plotted in Fig. 10 for visual comparison. Fig. 10 demonstrates that all the proposed modeling methods have a fast prediction speed. However, white-box modeling costs much less computation time than grey-box modeling and black-box modeling. The reason is that the prediction based on white-box modeling is by iterative computations through hydrodynamic coefficients and Eq. (17) and hence is the fastest; on the other hand, prediction based on grey-box modeling involves a high dimensional nonlinear input and hence costs a large amount of computation; although the input of black-box modeling is very simple, the RBF kernel function is quite memory- and CPU time consuming.

Table 4 Comparison of the prediction accuracy

Manoeuvres	Evaluation criterion	White-box modeling	Grey-box modeling	Black-box modeling
20°/20° zigzag	MSE	u: 3.0909×10^{-6}	u: 4.1396×10^{-5}	u: 4.25845×10^{-3}
		v: 6.1478×10^{-5}	v: 8.3322×10^{-4}	v: 1.0200×10^{-2}
		r: 5.2143×10^{-9}	r: 6.9638×10^{-8}	r: 8.0767×10^{-7}
		p: 1.2093×10^{-8}	p: 1.6670×10^{-7}	p: 1.7154×10^{-6}
	CC	u: 0.9999	u: 0.9999	u: 0.9981
		v: 0.9999	v: 0.9998	v: 0.9968
		r: 0.9999	r: 0.9997	r: 0.9962
		p: 0.9997	p: 0.9961	p: 0.9596
10°/10° zigzag	MSE	u: 1.4038×10^{-6}	u: 1.7008×10^{-5}	u: 2.4381×10^{-3}
		v: 7.6193×10^{-5}	v: 9.1550×10^{-4}	v: 1.4682×10^{-2}
		r: 5.8705×10^{-9}	r: 7.7978×10^{-8}	r: 1.1006×10^{-6}
		p: 5.0966×10^{-8}	p: 1.2304×10^{-6}	p: 7.6239×10^{-6}
	CC	u: 0.9999	u: 0.9997	u: 0.9814
		v: 0.9999	v: 0.9993	v: 0.9883
		r: 0.9999	r: 0.9989	r: 0.9850
		p: 0.9984	p: 0.96189	p: 0.7585
35° turning	MSE	u: 6.1803×10^{-8}	u: 7.7087×10^{-3}	u: 2.5632×10^{-1}
		v: 8.0514×10^{-7}	v: 4.8715×10^{-3}	v: 7.6885×10^{-3}
		r: 2.0996×10^{-12}	r: 8.9307×10^{-9}	r: 4.3855×10^{-7}
		p: 4.8442×10^{-11}	p: 1.8975×10^{-7}	p: 8.2096×10^{-7}
	CC	u: 0.9999	u: 0.9998	u: 0.9741
		v: 0.9999	v: 0.9917	v: 0.9697
		r: 0.9999	r: 0.9989	r: 0.9598
		p: 0.9999	p: 0.9741	p: 0.9381

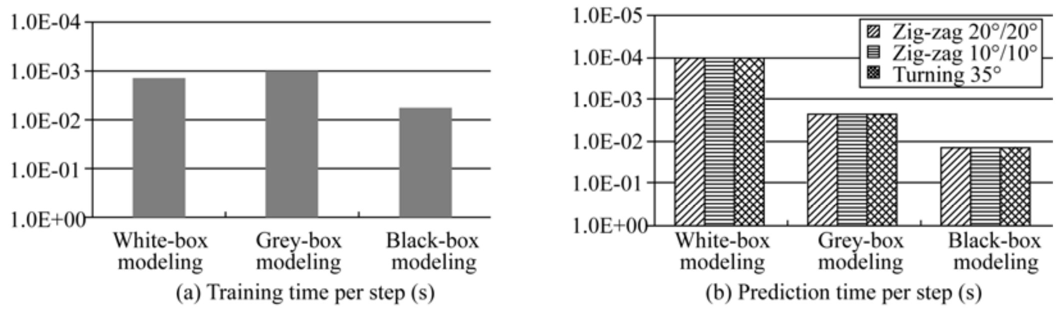

Fig. 10. Comparison of the prediction speed.

7. Conclusions

Based on LS-SVM, this paper has dealt with three system identification modeling methods for ship manoeuvring motion in 4-DOF, i.e., white-box modeling, grey-box modeling and black-box modeling. The conclusions can be summarized as follows:

(1) Good predictive ability and generalization performance of the proposed modeling methods are demonstrated by comparing the predicted results with those of simulation tests.

(2) Appropriate modeling method can be chosen according to the intended use of the mathematical models and the available data needed for system identification: When the hydrodynamic coefficients are to be determined, only white-box modeling should be chosen; when only the structures of the equations of ship manoeuvring motion is known, the gray-box modeling is a better choice; when both the principal ship parameters and the equations of ship manoeuvring motion are unknown, black-box modeling is the only choice for modeling of ship manoeuvring motion, but training samples from more manoeuvring types are needed.

(3) By comparing the MSE and CC between the prediction results and simulation data, it is shown that the accuracy of white-box modeling and grey-box modeling is significantly higher than that of black-box modeling.

(4) It is shown that all the modeling methods have fast prediction speed because of the SVM characteristics. In comparison, white-box modeling needs much less computation time than grey-box modeling and black-box modeling.

References

Abkowitz, M. A., 1980. Measurement of hydrodynamic characteristic from ship maneuvering trials by system identification, *SNAME Transactions*, **88**, 283–318.

Åström, K. J. and Källström, C. G., 1976. Identification of ship steering dynamics, *Automatica*, **12**(1): 9–22.

Bhattacharyya, S. K. and Haddara, M. R., 2006. Parametric identification for nonlinear ship manoeuvring, *J. Ship Res.*, **50**(3): 197–207.

Blanke, M. and Jensen, A. G., 1997. Dynamic properties of a container vessel with low metacentric height, *Transactions of the Institute of Measurement and Control*, **19**(2): 78–93.

Blanke, M. and Perez, T., 2002. *Mathematical Ship Modeling for Control Applications*, Technical Report, Technical University of Denmark.

Fossen, T. I., 1994. *Guidance and Control of Ocean Vehicles*, John Wiley & Sons Inc. New York, USA.

Haddara, M. R. and Wang, Y., 1999. Parametric identification of manoeuvring models for ships, *International Shipbuilding Progress*, **46**(445): 5–27.

Hayes, M. N., 1971. *Parameters Identification of Nonlinear Stochastic Systems Applied to Ocean Vehicle Dynamics*, Ph. D. Thesis, Massachusetts Institute of Technology.

Hess, D. and Faller, W., 2000. Simulation of ship manoeuvres using recursive neural networks, *Proc. 23rd Symposium on Naval Hydrodynamics*, Val de Reuil, France.

ITTC (International Towing Tank Conference), 2005. The manoeuvring committee final report and recommendations to the 24th ITTC, *Proceedings of the 24th ITTC*, Vol. 1.

Källström, C. G. and Åström, K. J., 1981. Experiences of system identification applied to ship steering, *Automatica*, **17**(1): 187–198.

Luo, W. L. and Zou, Z. J., 2009. Parametric identification of ship maneuvering models by using support vector machines, *J. Ship Res.*, **53**(1): 19–30.

Moreira, L. and Guedes Soares, C., 2003. Dynamic model of manoeuvrability using recursive neural networks, *Ocean Eng.*, **30**(13): 1669–1697.

Perez, T. and Fossen, T. I., 2011. Practical aspects of frequency-domain identification of dynamic models of marine structures from hydrodynamic data, *Ocean Eng.*, **38** (2-3): 426–435.

Rajesh, G. and Bhattacharyya, S. K., 2008. System identification for nonlinear maneuvering of large tankers using artificial neural network, *Appl. Ocean Res.*, **30**(4): 256–263.

Revestido, E. and Velasco, F. J., 2012. Two-step identification of non-linear manoeuvring models of marine vessels, *Ocean Eng.*, **53**, 72–82.

Rhee, K. P., Lee, S. Y. and Sung, Y. J., 1998. Estimation of manoeuvring coefficients from PMM test by genetic algorithm, *Proceedings of International Symposium and Workshop on Force Acting on a Manoeuvring Vessel*, Val de Reuil, France, 77–87.

Son, K. H. and Nomoto, K., 1982. On the coupled motion of steering and rolling of a high speed container ship, *Naval Architecture and Ocean Engineering*, **20**, 73–83.

Suykens, J. A. K. and Vandewalle, J., 1999. Least squares support vector machines classifiers, *Neural Processing Letters*, **9**(3): 293–300.

Vapnik, V. N., 2000. *The Nature of Statistical Learning Theory*, Springer Verlag, New York, USA.

Zhang, X. G. and Zou, Z. J., 2011. Identification of Abkowitz model for ship manoeuvring motion using ε-support vector regression, *Journal of Hydrodynamics*, **23**(3): 353–360.

Zhou, W. W. and Blanke, M., 1989. Identification of a class of nonlinear state-space models using RPE techniques, *IEEE Transactions on Automatic Control*, **34**(3): 312–316.